Length matters

Assecondi, Sara; Lavallee, Christina; Ferrari, Paolo; Jovicich, Jorge

DOI:
10.1016/j.jneumeth.2016.05.014

Document Version
Peer reviewed version

Citation for published version (Harvard):
Assecondi, S, Lavallee, C, Ferrari, P & Jovicich, J 2016, 'Length matters: Improved high field EEG-fMRI recordings using shorter EEG cables', *Journal of Neuroscience Methods*, vol. 269, pp. 74-87. https://doi.org/10.1016/j.jneumeth.2016.05.014

Title: Length matters: Improved high field EEG-fMRI recordings using shorter EEG cables

Author: Sara Assecondi Christina Lavallee Paolo Ferrari Jorge Jovicich

PII: S0165-0270(16)30102-9
DOI: http://dx.doi.org/doi:10.1016/j.jneumeth.2016.05.014
Reference: NSM 7532

To appear in: *Journal of Neuroscience Methods*

Received date: 27-11-2015
Revised date: 16-5-2016
Accepted date: 16-5-2016

Please cite this article as: Assecondi Sara, Lavallee Christina, Ferrari Paolo, Jovicich Jorge.Length matters: Improved high field EEG-fMRI recordings using shorter EEG cables.*Journal of Neuroscience Methods* http://dx.doi.org/10.1016/j.jneumeth.2016.05.014

Research Article

Length matters: Improved high field EEG-fMRI recordings using shorter EEG cables

Sara Assecondi[a,1], Christina Lavallee[a], Paolo Ferrari[a,2] Jorge Jovicich[a,*]

[a] Center for Mind/Brain Sciences, University of Trento, Rovereto, Italy

[*]Corresponding Author:

Jorge Jovicich

Center for Mind Brain Sciences

University of Trento,Via delle Regole, 101, 38100 Mattarello (TN), Italy

Email: jorge.jovicich@unitn.it

[1]Present address: School of Psychology, University of Birmingham, Birmingham, United Kingdom

[2] Present address: Azienda Sanitaria della Provinzia Autonoma di Bolzano, Bolzano, Italy

Highlights

- Concurrent brain EEG-fMRI recordings are challenging due to noise in the EEG signal
- We propose an EEG-fMRI setup aimed at reducing EEG noise at high MR fields
- Shorter EEG cables connect amplifiers force-locked to the MR-bed behind the RF coil
- Environment and MR-induced artifacts decreased by 60%, with low helium pump effects
- Implications for reproducibility, safety and ergonomics are discussed

ABSTRACT

Background: The use of concurrent EEG-fMRI recordings has increased in recent years, allowing new avenues of medical and cognitive neuroscience research; however, currently used setups present problems with data quality and reproducibility.

New Method: We propose a *compact* experimental setup for concurrent EEG-fMRI at 4 T and compare it to a more standard *reference* setup. The *compact* setup uses short EEG cables connecting to the amplifiers, which are placed right at the back of the head RF coil on a form-fitting extension force-locked to the patient MR bed. We compare the two setups in terms of sensitivity to MR-room environmental noise, interferences between measuring devices (EEG or fMRI), and sensitivity to functional responses in a visual stimulation paradigm.

Results: The *compact* setup reduces the system sensitivity to both external noise and MR-induced artefacts by at least 60%, with negligible EEG noise induced from the mechanical vibrations of the cryogenic cooling compression pump.

Comparison with Existing Methods: The *compact* setup improved EEG data quality and the overall performance of MR-artifact correction techniques. Both setups were similar in terms of the fMRI data, with higher reproducibility for cable placement within the scanner in the *compact* setup.

Conclusions: This improved *compact* setup may be relevant to MR laboratories interested in reducing the sensitivity of their EEG-fMRI experimental setup to external noise sources, setting up an EEG-fMRI workplace for the first time, or for creating a more reproducible configuration of equipment and cables. Implications for safety and ergonomics are discussed.

Keywords: concurrent EEG-FMRI; EEG cable length; multimodal neuroimaging; data quality; cryogenic pump noise

INTRODUCTION

Simultaneous recording of electroencephalographic (EEG) and functional Magnetic Resonance Imaging (fMRI) data (Ives, Warach, Schmitt, Edelman, & Schomer, 1993), although developed for clinical research (Hamandi, Salek-Haddadi, Fish, & Lemieux, 2004; Vulliemoz et al., 2011) has been extended to the cognitive neurosciences (H. Laufs et al., 2003; Helmut Laufs, 2008; Mulert & Lemieux, 2010; Ullsperger & Debener, 2010) as concurrent EEG-fMRI recordings have proven to be useful for studying brain functions with high temporal and spatial resolution, allowing both EEG and fMRI modalities to capture the same brain state simultaneously and providing the opportunity for a multitude of data-integration approaches (Huster, Debener, Eichele, & Herrmann, 2012). Obtaining quality EEG-fMRI data is, however, challenging due to severe degradation of the EEG signal, artifacts in the fMRI data (Goldman, Stern, Engel, & Cohen, 2000; Herrmann & Debener, 2008), as well as safety and data integration issues (Lemieux, Allen, Franconi, Symms, & Fish, 1997). Thus, it is important to optimize data quality at every step of acquisition and analysis, especially when considering analysis at the single-trial level (De Vos et al., 2013; Vanderperren et al., 2013).

The MRI scanner environment introduces several sources of noise contribution to the overall quality of the EEG signal. With different degrees of contribution to this noise, these sources include the strong static magnetic field (Allen, Josephs, & Turner, 2000; Debener, Mullinger, Niazy, & Bowtell, 2008; Goldman, Stern, Engel, & Cohen, 2000; Müri et al., 1998), the magnetic field gradient (Ertl et al., 2010; Felblinger, Debatin, Boesch, Gruetter, & McKinnon, 1995; Hill, Chiappa, Huang-Hellinger, & Jenkins, 1995; Ives, Warach, Schmitt, Edelman, & Schomer, 1993; Mandelkow, Halder, Boesiger, & Brandeis, 2006), the RF pulse (Anami et al., 2003; Garreffa et al., 2003; Lemieux, Allen, Franconi, Symms, & Fish, 1997; Mullinger, Debener, Coxon, & Bowtell, 2008; Negishi, Pinus, Pinus, & Constable, 2007), ventilation contributions (Nierhaus et al., 2013) as well as noise induced from the cryogenic cooling compression pump, which is often turned off during simultaneous EEG-fMRI recordings at high fields to reduce noise contributions (Kim, Yoo, & Lee, 2015; Mulert & Lemieux, 2010; Ritter & Villringer, 2006). On the other hand, MRI quality degradation occurs from the interference with EEG equipment, such as the gel (Mullinger, Brookes, Stevenson, Morgan, & Bowtell, 2008a). Additionally, the quality of simultaneously recorded EEG-fMRI data is highly dependent on the placement of EEG systems and the configuration of cables within the scanner (Chowdhury, Mullinger, & Bowtell, 2015), which may impact safety when electronic devices and conductive materials (i.e. EEG leads and electrodes) are in contact with the subject in the presence of strong magnetic fields (Lemieux et al., 1997). Furthermore, the placement of equipment and the participant is often not reproducible across laboratories, given the diversity of stimulus projection systems, EEG cable lengths, and interactions among instrumentation.

In order to address these aforementioned challenges in simultaneous EEG-fMRI acquisition, we designed and tested a *compact* EEG setup in a 4T MR scanner, whereby EEG cables were shortened and amplifiers were placed closer to the MR (RX/TX) coil and stabilized on a wooden form-fitting extension moving with the MR-bed. This configuration, which allows setup

of the whole system without having to access connections from the back of the magnet (thusly, involving handling of the back-projection screen for visual stimulation), was compared with a commonly used *reference* setup, which uses longer EEG cables connecting to the amplifiers placed inside the magnet from the back of the magnet bore. These two experimental setups were evaluated in terms of EEG sensitivity to MR-room environmental noise, degradation in both EEG and fMRI data due to cross-modality interferences, and sensitivity to functional responses elicited in a visual stimulation paradigm. Our results demonstrated that the *compact* setup achieves better EEG and comparable MR signal quality to the *reference* setup, without the need to modify existing MR-acquisition procedures (i.e. turning off the cryogenic pump or removal of the projection screen). We discuss the methodological benefit of the *compact* setup, as well as discuss implications for safety, ergonomics and reproducibility within the lab environment.

This work has been previously presented in preliminary form (Assecondi et al., 2013). To the best of our knowledge, prior to that conference proceeding, there are no reports of studies evaluating the effects of EEG cap cable shortening in simultaneous EEG-fMRI experiments. We discuss similarities and differences between our study and a recently published study that also demonstrated advantages of short EEG cables in concurrent fMRI at 7T (Jorge et al., 2015).

MATERIALS AND METHODS

Description of the Experimental Setups

The purpose of this study was to evaluate the quality of EEG and MR data from two experimental setups for simultaneous EEG-fMRI recordings (illustrated in Figure 1), which differed in the length of the EEG cables and the way in which the overall setup was mounted and therefore accessed by the experimenter.

MR-compatible EEG System. The EEG amplifier was a BrainAmp MR Plus modular amplifier (Brain Products GmbH, Gilchin, Germany) consisting of two MR-compatible units, of 32 unipolar channels each and an MR-compatible battery pack to both units (http://brainproducts.com). The MR-compatible caps had one electrocardiogram (ECG) channel and 63 EEG electrodes, arranged according to the 10-20 system, with leads arranged in two twisted bundles of cables. Electrodes were pin-type sensors, placed inside a plastic holder mounted on the cap, including a built-in resistor of 5 kΩ for EEG and 15 kΩ for ECG, plus 5 kΩ in the connector box. The electrode FCz was used as reference. The EEG cables terminated with two connector boxes, connected to the amplifiers using two ribbon cables. Two fiber optic cables connected the MR-compatible EEG amplifiers to the recording computer through the filter plate of the MR-room. EEG and MR scanner clocks were synchronized using EEG vendor "SyncBox" hardware to ensure consistent sampling (Mandelkow et al., 2006). Of note, both EEG setups had the same cap size (58 cm) and none of them used the EOG leads, which have been seen to significantly contribute to MR image artifacts (Mullinger et al., 2008b).

MR-Scanner. The MR scanner was a 4T MRI system (MedSpec, Bruker, Biospin head scanner with Siemens MAGNETOM electronics) with a birdcage transmitter and 8-channel receiver head RT coil (USA Instruments), which is particularly suitable for EEG recording since it has a hole at the top of the head in correspondence with the exit point of the EEG leads.

Reference setup. In the *reference* setup, depicted in Figure 1 (upper panel), EEG amplifiers were placed inside the magnet bore, at the back, which, in our laboratory, required the removal of the projection screen, placed on the back of the magnet. The amplifiers were positioned to the left and right side of the power pack to avoid obstructing the subject's view of the projection screen and were stabilized with weighted sand bags. The cables, connecting the cap and the amplifiers were

thus forced to be misaligned with respect to the z-axis of the magnet, and had an approximate length of 111cm (EEG leads ~ 16cm from FT10 to Cz plus ~ 65cm from Cz to connector, ribbon cables ~ 30cm). This misalignment is impossible to avoid with the *reference* setup when two amplifiers are used in combination with a back-projection screen in order to guarantee sufficient visibility of the stimuli. The EEG cables were connected to the amplifiers only after the subject, with the EEG cap and the MR-coil in position, was moved along the MR-bed into the magnet. The back-projection screen was then remounted on the back of the magnet bore.

Compact setup. The *compact* setup, depicted in Figure 1 (lower panel), was comprised of an in-house constructed wooden bed extension and a modified MR-compatible EEG cap. The amplifiers and power pack were placed onto the form-fitting wooden extension, force-locked to the back of the MR patient bed, with the amplifiers stacked one above the other, with the bottom one flipped upside down, and the power pack behind them. By flipping the bottom amplifier, we ensured a straight, parallel routing of the cables and connectors, with minimal misalignment from the z-axis of the magnet. The extension was fitted along the inner profile of the magnet bore and slid back and forth inside the bore, together with the MR-bed and fiber optic cables. This *compact* setup enabled the use of a modified (kindly executed by Brain Products) MR-compatible cap with shorter connecting cables of an approximate length of ~46cm (EEG leads ~ 16cm from FT10 to Cz plus ~9cm from Cz to connector, ribbon cables 21 cm), such that the cables fell straight along the z-axis of the magnet bore. The amplifiers and cables were stabilized with weighted bags. The proximity of the amplifiers to the MR-coil assured full visibility of the back-projection screen even with the stacked amplifier configuration. This *compact* setup allows the operator to connect the amplifiers to the EEG cap when the MR-bed is still outside the magnet bore, which is not only more time efficient, more comfortable for both the subject and experimenter, but is also fully reproducible across experiments.

Identification of Laboratory Noise Sources in EEG Signals

To identify possible sources of environmental noise impacting the EEG signal measured inside the MR scanner, we systematically turned off and on devices routinely used in the MR laboratory and recorded four minutes of phantom EEG with the reference setup. For comparison, four minutes of phantom data were also recorded with the scanner in stand-by, whereby all relevant electronics were switched off. These devices included: the headphone system, ventilation system inside the magnet bore, the camera at the back of the magnet bore, the MR-room ventilation system and the MR-scanner cryogenic pump. The power spectral density (PSD) was calculated for each recording and device (Hamming window, spectral resolution 0.1Hz) and was compared with the stand-by recording. Noise sources were identified as coming from devices eliciting unexpected PSD frequencies, relative to the stand-by condition, for which a PSD profile was expected to be dominated by flat noise and without large unexpected peaks.

Human subjects and visual stimulation

Two healthy volunteers (female, 26 and 29 years old), without history of psychiatric, neurological or systemic disease, participated in this study approved by the ethics committee of the University of Trento. Subjects were right handed and had normal or corrected to normal vision. The visual task consisted of passively viewing a pattern-reversing checker-board (4 Hz) in alternating cycles of 10 s of fixation and 20 s of stimulation, for a total of 1200 trials (1 trial = 1 presentation of the checker-board). The stimuli were projected on a semi-opaque screen, placed at the end of the magnet bore, and watched by the subjects via a mirror mounted on the top of the MR RF-head coil (visual angle 18^{o}x15^{o}) The stimulation was programmed with MATLAB Psychtoolbox-3 (Brainard 1997) for Windows. There were differences in the effective visual FOV between the two EEG-

fMRI setups. In the CMP setup, the proximity of the EEG amplifiers to the back of the head RF coil was such that it caused no visual obstruction to the projection screen (Fig. 1).

Acquisition Parameters

The acquisition parameters described in the following section were applied to both phantom and human recordings.

EEG Recordings. The EEG signal was recorded from 63 EEG channels and 1 ECG channel with a 5000Hz sampling rate.

MRI Recordings. Anatomical MRI was acquired using a 3D Magnetization-Prepared Rapid Gradient Echo (MPRAGE) sequence, optimized for gray-white matter contrast (TE 4.18ms, TR 2700ms, TI 1020ms, flip angle 70˚, 1mm isotropic voxels, 256x224 matrix, 176 sagittal-oriented slices, Generalized Autocalibrating Partially Parallel Acquisition acceleration factor 2) (Papinutto & Jovicich, 2008). Two repetitions of the fMRI protocol were acquired for each subject and condition. A standard full-brain single shot gradient echo 2D Echo-Planar Imaging (EPI) protocol (TE 22ms, TR 2200ms, flip angle 75˚, 3mm isotropic voxels, 64x64 matrix, 37 axial AC-PC-oriented slices, slice gap 0.45mm, 180 volumes) was used. The point-spread function (PSF) distortion correction method was used for EPI data (Zaitsev, Hennig, & Speck, 2004; Zeng & Constable, 2002). Static field (B_0) maps were derived from a double-echo gradient sequence (TE 6 and 10ms, TR 400ms, flip angle 39˚, 2mm isotropic voxels, 128x128 matrix, 75 sagittally-oriented slices, slice gap 0.3mm, fat saturation) (Jezzard & Balaban, 1995; Robinson & Jovicich, 2011). B1 field maps were derived from double flip angle Turbo Spin Echo sequence (TE 18ms, TR 6000ms,

flip angles 60˚ and 120˚, 0.86 x 0.86 x 5mm voxels, 256x256 matrix, 30 sagittally-oriented slices, slice gap 0.75mm) (Morrell, 2008).

Temperature Measurements. As a safety concern to detect potentially harmful temperature increases, we monitored temperature fluctuations during phantom recordings with four MR-compatible temperatures probes (LumaSense Technologies, Santa Clara, CA) at four electrode positions (ECG, REF, Cz, Oz), as those locations are where the distribution of the EEG lead is denser (Angelone et al., 2006) and the risk of excessive heating is higher (Lemieux et al., 1997). The probes were placed inside the plastic holder of a subset of electrodes, deep in the conductive gel, as close as possible to the pin-type sensor. Temperature was measured at 1Hz and referenced to room temperature.

Controlling Subject and Phantom Positions. Previous studies have shown that fMRI-induced artifacts in the EEG signals can depend on the position of the sample in the RF coils along the main axis of the magnet (Mullinger et al., 2011). Therefore, considering that one of the main goals of this study is to compare the phantom and human EEG-fMRI recordings under different experimental conditions, it was important to minimize differences that could solely arise from the positioning of the subject. Towards this end, phantom position variations were minimized by using a purpose-built phantom holder that fits tightly inside the head RF coil. Standard landmarking procedures that align the eyebrows of the subject with the center of the head RF coil and center of the magnet were used.

Phantom Recordings

The EEG cap was placed on a spherical silicon oil phantom (170mm diameter), which had been previously covered in a thin layer of conductive gel (Abralyt 2000). The electrodes were filled with the same gel (total gel used 60ml) to achieve electrode impedances below 5kΩ. We placed the ECG

below the right-frontal electrode (2cm below Fp2, with the lead folding around the left side of the phantom from the back to the front) to maximize the reproducibility of the position of electrodes and wires across sessions.

Artifacts Induced on Phantom EEG. In our lab, the cryogenic pump and MR-room ventilation system (see above) were the strongest sources of environment noise sources affecting the EEG signal when fMRI data were not simultaneously acquired. Thus, we were able to investigate the individual and combined contributions of only these two noise sources on the EEG signal. We recorded 5 minutes of phantom EEG under the four conditions, with (IMG) and without (STATIC) concurrent fMRI recording, on both experimental setups (Tables 1 and 2).

Artifacts Induced on Human EEG. With both (*compact* and *reference*) setups, we compared two combinations of environmental noise conditions as previously defined for the phantom experiments with both the cryogenic pump and the MR-room ventilation system on and functioning (ALL-ON), which corresponds to the standard working condition of the MR-scanner and the least ideal condition for the EEG system, as well as with both the pump and ventilations system switched off (ALL-OFF), corresponding to the most ideal condition for the EEG system. Each condition was repeated with (IMG) or without (STATIC) concurrent fMRI acquisition.

Artifacts Induced on Human MR Images. With both setups, we compared several image sequences (structural MRI, functional MRI, B_0, and flip angle maps) during sessions of concurrent EEG-fMRI (EEG) and the session of pure fMRI in the absence of EEG equipment (MRI).

Data Analysis

EEG Signal Analysis. EEG data were analyzed with BrainVision Analyzer 2.0 (Brain Products GmbH, Gilching, Germany), EEGLAB (Delorme & Makeig, 2004) and in-house developed Matlab code (Mathworks, Natick, Massachusetts, USA). We evaluated the following aspects of EEG data quality: influence of the experimental setup on artifacts induced on EEG by environmental noise (ventilation system of the MR room and cryogenic pump of the magnet), influence of the setup on artifacts induced on EEG by fMRI, and influence of the setup on task-related event-related responses (ERPs).

Influence of the Setup on Artifacts Induced on EEG by Environmental Noise. For this analysis, phantom EEG data recorded with concurrent fMRI were not considered since the superimposed MR-imaging artifacts make it difficult to identify the external noise sources. Apart from the hardware 250Hz low-pass filter, PSD (Welch periodgram, Hamming window, spectral resolution 0.1Hz) and the maximum PSD envelope (i.e. the maximum across EEG channels) were calculated on raw EEG data without additional filtering or downsampling. We visually inspected the PSD profiles in different conditions (EEG-ONLY: ALL-ON, ALL-OFF, PUMP-ON,VENT-ON), with reference to the ALL-OFF condition, to identify frequencies specific to contaminating noise sources (i.e. the cryogenic pump and the ventilation system). To quantify the contribution of the various noise sources, the total power was calculated and plotted topographically. For each condition, we also calculated and reported the average total power reduction across channels, calculated as $(PSD_{REF} - PSD_{CMP})/PSD_{REF}*100$. The ECG was analyzed separately using the same procedure.

Influence of the Setup on Artifacts Induced on EEG by Concurrent fMRI. To address the influence of experimental setup on EEG during concurrent EEG-fMRI, we analysed phantom EEG data in the ALL-ON condition. These recordings only contain the imaging artifact and external noise,

depending on the condition (see Table 1). Raw EEG data was segmented around triggers indicating the MR-volume in epochs of 2210ms (-10ms before the onset; one TR=2200ms), baseline corrected with respect to the pre-stimulus period, and averaged to obtained an average MR-volume artifact, as well as its standard deviation (SD) across volumes. The root-mean-squared (RMS) values of both amplitude and SD of the average MR-volume artifact (Mullinger et al., 2011) were calculated both before and after artifact removal in order to quantify its strength and variability. This procedure was iterated for each channel and represented as a scalp distribution. We also calculated and reported the average RMS reduction of the SD across channels, calculated as $(RMS_{REF} - RMS_{CMP})/RMS_{REF}*100$.

Influence of the Setup on ERP. We reduced the imaging and ballistocardiogram MR-related artifacts in human EEG recordings using an Average Artifact Subtraction (AAS; Allen et al., 1998, 2000) technique, as implemented in BrainVisionAnalyzer 2.0 and, with Matlab, was further filtered (0.16Hz -40Hz), downsampled to 250Hz, segmented around markers which indicated reversal of the checkerboard in epochs of 300ms (-50ms before the stimulus) and baseline corrected with respect to the pre-stimulus period. Epochs with absolute amplitude exceeding a given threshold were removed (threshold of 150 uV on each EEG channel for large movements and 70uV on FP1 and FP2 for eyeblinks). We then calculated averaged ERPs (ALL-ON, ALL-OFF; both STATIC and IMG conditions) at Oz based on the expected occipital positive deflection at roughly 100ms (P100) post-stimulus (Odom et al., 2004, 2010). Scalp maps at the P100 latency were inspected for each condition.

MR Image Analysis

MR data were analysed with in-house developed Matlab code and FSL (www.fmrib.ox.ac.uk/fsl/ (Smith et al., 2004; Woolrich et al., 2009)). Two aspects of MR-data quality were inspected:

influence of the setup on the quality of MR-images (phantom and human recordings) and influence of the setup on fMRI activations (fMRI recordings on two human subjects during a visual task).

Influence of Setup on the Quality of the MR-images. To characterize artifacts in the MRI data due to the presence of the EEG equipment in the magnet bore, for the two experimental setups the following three sessions were considered during the acquisition of functional MRI data: whole EEG system in place and recording in the magnet bore (EEG-full), only the EEG amplifiers and battery pack placed in the magnet bore and switched off (EEG-amps) but without the EEG cap, and no EEG system present in the magnet room (EEG-none). We inspected structural and functional images to identify distortions. Additionally, functional images were analyzed in correspondence with the FBIRN quality assurance protocol (Friedman & Glover, 2006) and were compared under the various conditions and experimental setups with FBIRN means and SDs collected in our lab over the past three years in the same MR-scanner without any EEG equipment. Human MRI data underwent the same FBIRN quality assurance protocol after motion corrections (functional) and co-registration (structural) procedures were calculated. Structural images were also compared before and after brain extraction (Smith, 2002), to assess whether possible distortions could reach the brain beneath the scalp.

To disentangle the relative contribution of B_0 and B_1 inhomogeneity to MRI data quality, we calculated maps of the static field on the flip angle α. Maps of the static field (B_0-maps in Hz) were obtained as a scaled difference between the phased images obtained by each echo as $\Delta B_0=(2\pi y \Delta T\, E)^{-1}\Delta\Phi$ (Jezzard & Balaban, 1995), after phase unwrapping (Jenkinson, 2003), where y is the gyromagnetic ration, $\Delta T\, E$ is the difference between echo times and $\Delta\Phi$ is the difference between phase images. We visually inspected the B_0 maps and compared them across various experimental setup conditions (EEG-full, EEG-amp, EEG-none session, *reference* vs *compact*), for both phantom and human recordings. Maps of the flip angle were calculated on a voxel basis as α

$=\arccos \sqrt[3]{M_2/8M_1}$ (Morrell, 2008), where α is the flip angle, M_1 and M_2 are the acquisition intensities at the voxel from the two different flip angles. The α-maps were normalized to the average flip angle within a central ROI of 30 voxels, and visually inspected for both human and phantom data. The SD of the B0 and normalized flip angle α were calculated for each slice for the three setups: CMP, REF and EEG-none. The comparison of inhomogeneities across experimental conditions (CMP vs. EEG-none, REF vs. EEG-none, CMP vs. REF) was done using a two-tailed paired t-test across slices.

Influence of the Setup on fMRI Activations. Using a single-subject General Linear Model (GLM) analysis, as implemented in FSL, we derived fMRI activation maps. fMRI data were motion-corrected, spatially smoothed with a 5mm kernel and analyzed using a gamma HRF plus temporal derivatives. The first five initial volumes were discarded to allow for signal stability. Statistical maps were threshholded using clusters of Z>2.3 and a (corrected) cluster significance threshold of p=0.05 (Worsley, Evans, Marrett, & Neelin, 1992).

Results

Unless otherwise stated, all error measures are standard deviations.

EEG Signal Quality

Influence of the setup on artifacts induced on EEG by environmental noise. The MR-room ventilation system and the cryogenic pump introduced major noise sources on the *reference* setup without concurrent fMRI (STATIC); whereas, the headset, magnet bore ventilation system and camera did not introduce any characteristic frequency in the PSD profile. The characteristic frequencies of the MR-room ventilation system (VENT-ON) and cryogenic pump (PUMP-ON) were identified by comparing PSDs to the ALL-OFF condition in both setups. The upper row of Figure 2 shows the maximum envelopes of the PSD profiles, which were normalized to their

respective maximum, for EEG channels (STATIC: VENT-ON, PUMP-ON, *compact* vs *reference*). Despite some relative amplitude differences within each condition (VENT-ON and PUMP-ON), the contaminating frequencies appear quite similar in both setups. The lower row of Figure 2 displays the scalp distribution of the total PSD, whereby the absolute value of the total power contribution due to the ventilation system and cryogenic pump is much stronger in the *reference* than in the *compact* setup (average total PSD reduction across EEG channels: 85 ±19% in ALL-ON, 67 ± 35% in VENT-ON and 84 ± 20% in PUMP-ON). The Cz channel, corresponding to the point where the EEG lead bundles leave the cap, is more sensitive to noise in the *reference* setup than in the *compact* setup.

To summarize, phantom EEG experiments with no concurrent fMRI demonstrated that the *compact* setup is much less sensitive to EEG signal noise introduced by the magnetic room ventilation system and cryogenic pump, with a power spectrum density reduction of about 85% relative to the noise level of those sources in the *reference* setup.

Influence of the setup on artifacts induced on EEG by concurrent fMRI. Scalp distributions (Figure 3) of RMS values for the two experimental setups before and after artifact removal indicate a smaller RMS in the compact as compared to the reference setup in phantom recordings. RMS values in the reference setup (Figure 3) are highest at Cz; whereas, in the compact setup, these values are highest at the back of the head. In the reference setup, the electrodes affected by high variability of the artifact were the same in all conditions (ALL-ON, ALL-OFF, PUMP-ON, VENT-ON). In the compact setup, we found that the same electrodes showed high artifact variability (i.e. RMS) in the ALL-ON and PUMP-ON conditions, and in the ALL-OFF and VENT-ON conditions, respectively (not shown). The EEG artifact variability, quantified as the RMS of the artifact mean or SD, was systematically smaller in the compact setup (Supplementary Table 1). In particular, for

the ALL-ON condition after AAS pre-processing, the noise reductions were approximately 78% and 68 % for the RMS mean and RMS standard deviation, respectively.

Thus, phantom EEG experiments with concurrent fMRI, showed that relative to the reference setup, the compact setup offered over 60 % reduction in EEG signal variability in the condition ALL-ON after data preprocessing.

Influence of the setup on ERPs. Simultaneous EEG-fMRI data was collected on subjects (N=2) during a visual task for both the *compact* and *reference* setups. Artifact-corrected (AAS preprocessed and ballistocardiogram corrected) ERPs to the passive viewing of a flashing checkerboard are depicted in Figure 4 with cryogenic pumps and ventilation systems on (ALL-ON). These ERPs are consistent with the expected (P100) patterns of activation both in space (upper row: bilateral occipital activation) and time (lower row: 100ms post-stimulus peak) (Odom et al., 2010). Similar patterns were identified for both subjects, regardless of the condition (ALL-ON, ALL-OFF; STATIC or IMG; data not shown).

The P100 amplitude was higher in the *compact* than in the *reference* setup for both subjects (subject 1, in Figure 4, IMG-ALL-ON: 11.88±0.82μV in *compact*, 8.35±0.62 in *reference*; IMG-ALL-OFF: 11.25±0.86 in *compact*, 10.20±0.47μV in *reference*; subject 2 IMG-ALL-ON: 12.65±0.34 in *compact*, 10.73±0.32 in *reference*; IMG-ALL-OFF: 12.4±0.34 in *compact*, 9.66 ±0.29 in *reference*).

In summary, human ERP data obtained concurrently with fMRI showed that: i) the ERP amplitudes of the *compact* setup do not significantly change between environmental noise conditions, whereas for the *reference* setup the ERP amplitudes are significantly reduced in standard environmental conditions (cryogenic pump and ventilation systems on); and ii) the ERP signals are higher for the *compact* relative to the *reference* setup, suggesting a higher sensitivity and potentially higher SNR, which may extend to the single-trial level.

MR Image Quality.

Influence of the Setup on the Quality of MR-images. Regardless of whether EEG equipment was removed from the scanner (EEG-none) or only the amplifier and battery were present (EEG-amp), we found the quality of MR-images to be comparable. Furthermore, with all EEG equipment (EEG-full) present, the ON/OFF combinations of the cryogenic pump and MR room ventilation systems did not affect MR-image quality. Thus, for brevity, we present only the comparison of MRI data acquired with and without the EEG equipment (EEG-full vs EEG-none), ALL-ON across experimental setups.

Anatomical MRI Data. Figure 5 shows one representative slice of MPRAGE images (single subject, phantom data), with and without brain extraction. In human data, indentations on the scalp, due to electrodes and conductive gel are visible in both the compact and reference setup (upper row); however, not in the brain-extracted data (middle row). The presence of the EEG does affect the anatomical image intensity homogeneity with respect to the pure MRI condition (i.e., no EEG equipment, EEG-none), but does not affect the quality of the brain segmentation. Phantom data were less prone to signal dropout. Figure 6 shows the percent difference maps of the anatomical images in each EEG setup (CMP and REF) relative to the EEG-none condition [(CMP - EEG-none)/EEG-none and (REF - EEG-none)/EEG-none], for one sample subject. The general pattern found was that the CMP setup increased the image intensity of anatomical images in the frontal areas whereas the REF setup increased the signal in the superior areas. None of the EEG setups produced visible distortions.

Functional MRI Data. The FBIRN stability parameters (Friedman and Glover, 2006) changed with respect to the baseline condition of EEG-none (i.e. no EEG equipment) regardless of the

experimental setup (see Table 3). Average signal intensity, SD, drift increases while SNR, signal-to-fluctuation noise ratio (SFNR) decreased when the EEG cap was on. In all cases, except for the average signal intensity, the effects of the EEG cap remained within 2 SD from the baseline equipment (no EEG equipment). Further, we did not find any structured noise in the summary stability images from phantom and human data (supplemental Figure S1). In summary, as with the anatomical MRI the fMRI data is of comparable quality on both EEG-fMRI setups.

B_0 and Flip Angle Maps. Figure 7 shows a central sagittal slice of functional, B0, and flip angle maps for phantom recordings with simultaneous EEG recordings (CMP: compact, and REF: reference) and without EEG equipment in the magnet (EEG-none). Image distortions in proximity to the EEG electrodes positions are evident on the surface of the phantom EPI and B0 images, and less so in the EEG-none EPI data. Spatial inhomogeneities in B0 are present for all conditions whereas flip angle maps are homogenous across conditions. Qualitatively, the B0 inhomogeneities in the phantom MR data are visibly more pronounced in two EEG configurations relative to the EEG-none condition, particularly at the surface of the phantom in proximity to the electrodes (Figure 7). The B0 differences between the CMP and REF conditions appear to be less strong, and might depend on the amount of gel present, which was kept similar to the amount used in human recordings but was hard to control. A quantitative analysis based on the SD average across the full phantom volume in B0 and flip angle shows consistent inhomogeneity results, higher image uniformity in the EEG-none condition relative to the two EEG-fMRI setups (Fig. 7, Table 4). The REF setup gave significantly larger flip angle inhomogeneities than the CMP. Both setups distorted the static B0 field similarly (Table 4). Qualitative evaluations on human data show similar results (Supplementary Figure S2).

Influence of the Setup on fMRI Activations. Functional activations in response to a visual paradigm are concentrated around occipital regions (Figure 8), whereby the same occipital activation was derived for both setups in the simple sensory task.

Temperature Measures. The temperature curves, with reference to room temperature, for the phantom recordings (Figure 9), demonstrated no abnormal trends regardless of the imaging sequence considered.

Discussion.

In this study we propose a compact EEG-fMRI setup characterized by shorter connecting cables mounted on a form-fitting MR bed extension. With phantom experiments we demonstrate that, relative to a standard reference setup with longer cables, the compact setup significantly reduced the effects of external noise sources on the EEG while maintaining overall similar MRI quality across EEG-fMRI setups. As a proof of concept, we demonstrate similar effects on two healthy volunteers, with improved visual ERP responses of the compact setup relative to the reference setup, while maintaining comparable MRI quality. Given that this setup reduced user interaction, we discuss its implications in improving reproducibility across experiments, as well as safety and ergonomic concerns in the workplace.

EEG Quality

The cryogenic pump and MR-room ventilation system were identified as the two major sources of environmental noise in our MR laboratory setting. In the *reference* setup, electrodes most affected by the cryogenic pump were those located at the exit point of the cable bundles from the EEG cap, most likely because the longer EEG cables in the *reference* setup are more difficult to stabilize and therefore more prone to scanner vibrations. On the other hand, in the *compact* setup, we employed

shortened cables allowing for easier stabilization of the bundles, thereby reducing the effect of vibrations. Moreover, shorter cables are less prone to artifacts caused by the imaging process.

Shortening of the EEG cables has also proven to be effective in higher scanner field (7T) laboratories (Jorge et al., 2015). In fact, our study has several similarities and differences in comparison to this recent study. The main similarities are that both studies found the same main effects: shortening the cables significantly reduced the noise contributions of the helium pump in the EEG signal, and also gave clear EEG visual evoked responses in a study with a few healthy volunteers. Another similarity is that both studies, being at high fields (> 3T), evaluated heating related safety aspects concluding no increased risks with the shorter EEG cable setups proposed. Both studies used 64 channel MR-compatible equipment modified from the same vendor (Brain Products), with a similar setup of EEG cables leaving the head RF coil from its open back aperture. Differences between the two studies include the field strength (our study 4T, theirs 7T), cable lengths tested (our study 9 and 65 cm, theirs 12, 50 and 100 cm), cable arrangement (ours was always flat, while Jorge et al tested bundled and flat arrangements), number of healthy subjects and sessions with visual stimulation (our study scanned 2 subjects in three sessions each, using the two EEG setups and none, their study scanned 5 subjects one session each, using the shortest cable setup), and wooden support for amplifiers (while both are always at the same position relative to the central axis of the bore during acquisition, ours was coupled to the table bed, theirs is not). Although both studies looked at the effects of EEG-fMRI setup on MRI quality, our study focused on the comparison between the two experimental setups tested (short vs long EEG cable) and showed that MRI quality was to a large degree preserved across the EEG-fMRI setups. Jorge et al., 2015 focused their comparison between their shortest cable EEG-fMRI setup and no EEG cap, clearly showing big differences, as expected. Another important difference in our study is that we directly compared EEG visual evoked potentials measured separately in the two cable setup configurations, showing indicative improvements with the short cable setup. Of note, in both

studies ERP measures were obtained while the helium pump was normally functioning. Clearly, with just two subjects our ERP results are only indicative. Jorge et al (2015) offer a better characterization with more subjects while always using the shortest cable setup (i.e., no ERP comparisons across experimental setups are available). Using phantom data, both studies show that the helium pump contributes significantly to EEG signal noise, particularly in the 20-150 Hz range. With the helium pump on, our phantom study measured 85% EEG noise reduction when using the shorter cable setup in a 5 minute interval, while Jorge et al., 2015 measured an improvement of 58-62 % with their shorter cable setup in a 30 second interval. Therefore, despite the various experimental differences both studies show consistent and complementary evidence that, at high fields, there is an advantage in using short EEG cables in simultaneous EEG-fMRI studies.

Phantom EEG data measured during concurrent fMRI suggests that the stabilization of cables in the compact setup provided an advantage when correcting EEG data for MR-gradient artifacts, as employed with AAS techniques. Regardless of environmental conditions (ALL-ON, VENT-ON, PUMP-ON, ALL-OFF) the compact setup always showed a significant reduction in the variability of EEG noise power. AAS approaches, by definition, subtract an artifact template containing only the deterministic part of the artifact (not its variability). The residual variability in the data determines the SNR of the cleaned EEG. The higher variability introduced in the reference setup would lead to worse SNR, when AAS techniques are used. Therefore, the compact setup is advantageous because of its stabilizing effects on the electrodes, which result in a reduced contribution from the helium pump and less variability in the MR artifacts induced in the EEG signal, thus leading to enhanced EEG SNR after artifact removal.

Human recordings during a visual stimulation task yielded scalp maps and ERPs in line with previous literature; however, P100 amplitudes were higher in the *compact* than *reference* setup across subjects and conditions (ALL-ON, ALL-OFF, sessions randomized). Although this may suggest enhanced SNR achieved with the *compact* setup, an extended dataset and single trial

analyses, which is beyond the scope of this paper, should be conducted to verify this claim, as averaging the signal only captures part of the data. It may be reasonable to assume that reduced contaminating frequencies within the *compact* setup lead to improved signal quality for single-trial analysis, which is of importance for multimodal EEG-fMRI integration (Huster et al., 2012; Lavallee, Herrmann, Weerda, & Huster, 2014).

MRI Quality

In addition to assessing EEG signal quality, we also assessed MR image quality, which was in general comparable in both EEG setups, likely due to the presence of electrodes and gel (conductive materials).

B0 and flip angle maps provided information on the sources of signal loss and image distortion due to inhomogeneity in the static magnetic field. Consistently with previous high field studies, we found that both concurrent EEG-fMRI setups introduce B0 and flip angle inhomogeneities relative to the EEG-none condition (Mullinger et al., 2008b). We found that the B0 inhomogeneities were similar in both setups, but that the REF setup introduced higher flip angle variability, potentially due to the stronger interference from RF signals induced on the longer EEG cables during the imaging process. Both setups gave image intensity inhomogeneities in the structural images, yet none of the two EEG-fMRI setups gave visible signal loss distortions in proximity to the electrodes, neither in structural nor functional MRI. A qualitatively comparison with previous EEG-fMRI 3T results (Mullinger et al., 2008b) suggests that our setups gave slightly lower image distortions, despite the fact of having used a slightly higher static field of 4T. Several important experimental differences may help explain these differences. Our study did not use EOG wires, so B1 effects from this source were not present. Our study used pin electrodes, which have less conductive elements than the ring electrodes used by Mullinger et al., 2008b. Further, our study used a head transmit RF coil, whereas the 3T experiment of Mullinger et al., 2008b used a

whole body RF coil. The combination of these experimental differences may have played a role to make our EEG-fMRI experimental setups less sensitive to B0 and RF effects in the MRI data.

Summarizing the MRI quality evaluation, by using the compact setup, we have successfully reduced variability in the artifacts seen in EEG data, without severely compromising structural or functional fMRI quality.

Safety

In this manuscript, safety aspects were evaluated from three perspectives. The first safety criteria was based on phantom surface temperature measurements during the acquisition of MRI data that would be used in a typical fMRI study, as has been done by other studies for the evaluation of local heating risks (Lemieux et al., 1997; Mullinger et al., 2008; Jorge et al., 2015). Our phantom temperature measures, lasting approximately one hour, showed no abnormal temperature increases in either EEG setup, suggesting that both the compact and reference setups behaved similarly. A limitation of this study is that the temperature measures in each setup were done only once.

The remaining safety criteria did not involve measurements, but rather practical and theoretical considerations. The second safety criteria was based on efficient access to the subject inside of the scanner, which is accomplished easily and more quickly with the compact than with the reference setup as the compact setup is fixed to the MR-bed and does not require additional removal of a back-projection screen (as in the reference setup) to access EEG connectors. The third safety concern was based on the length of EEG cables, as burning hazards are a known risk when electronic devices are connected to the subject in the MR environment. When the length of cables approximate half the wavelength of the resonant frequency, energy is absorbed by the cable and is confined to the vicinity of the electrode (standing wave effect), thus acting like an antenna (Dempsey et al., 2001), possibly leading to a higher risk of burning the subject. The resonance frequency, v, increases with magnetic field strength while the corresponding wavelength (λ)

decreases, meaning that higher fields correspond to a shorter resonant length (see Table 5 for examples); however, shorter EEG cables correspond to improved EEG signal quality. These aspects should be considered when the reference setup is modified, as our compact setup employed a 25 cm cable length, which is below the resonant length of up to 7T. Thus, the compact setup may be used in up to a 7T scanner, as has actually been already demonstrated (Jorge et al., 2015). It is also of critical importance that this antenna-like effect is dependent on the position of wires within the bore, being worse when the cables are far from the center (interaction with inhomogenous RF). The configuration of the compact setup provides another advantage over the reference setup, as the cables fall straight along the z-axis, minimizing possible standing-wave effects.

Summarizing, from a safety point of view and with respect to the *reference* system, the *compact* system did not show increased risks of local heating. While not directly measured, the *compact* system may offer some advantages related to practical ease of access to subject and shorter cables being a less efficient antenna that can increase energy in the electrode.

Reproducibility

The experimenter plays a crucial role in the reproducibility of any experimental setup. Simplifying an experimental setup by offering less freedom to the operator is expected to reduce the probability of setup variability, therefore increasing the level of reproducibility. The commonly used *reference* setup provides a great deal of freedom for placing the cables and the EEG system, which is highly disadvantageous as it not only compromises the reproducibility of the experimental setup across acquisitions, but also the position of EEG cables inside the magnetic field effects both the imaging and the ballistocardiogram effect. By using the *compact* setup, amplifiers are fixed on a wooden extension and very short EEG cables, the operator is not given excessive freedom in the placement of the system inside the MR-scanner, which is a major advantage to operators who do not have much experience in the field of both EEG and fMRI recordings. Additionally, by using an

RF(RX/TX) head coil that is open at the back, EEG cables could exit from the coil in an almost straight line towards the amplifiers at the back of the coil, reducing degradations to the signal that may occur from misalignment to the z-axis. Although it was not tested within this paper, it may still be possible to use the *compact* setup with an RF (RX/TX) head coil that is closed at the back; however, although this might degrade the overall performance of the system (due to misalignment), the main advantages of the proposed setup (i.e. stability of cables and amplifiers, better SNR of EEG, reproducibility of the EEG placement, safety) are nonetheless to be retained. Furthermore, this *compact* setup, which offered a clear improvement in data quality, safety and ergonomics of the whole EEG-fMRI workplace, can be adapted to different scanner platforms and to other MR-laboratory configurations, providing portability and reproducibility across testing facilities.

A different aspect of reproducibility refers to potential differences between the compact and reference setups that are strictly related to EEG cap differences, unrelated to the cable length differences. By construction, the comparison of the two proposed setups required, in our case, the use of two different EEG caps. The caps, however, were of the same size, number of channels and vendor. The cap mounting was always done by the same researcher following the same described procedures. Therefore, even if we tried to minimize differences unrelated to cable length, these cannot be ruled out and could in principle bias the results in any way. However, our main findings are in good agreement with those of other similar studies (Jorge et al., 2015), therefore suggesting that the main effects are driven by cable length differences.

Conclusions

By presenting the *compact* setup, we have highlighted how the careful choice of EEG setup offers a clear improvement in data quality, as well as safety (in terms of ergonomics and ease of access) and reproducibility of the EEG-fMRI workplace. The use of the *compact* system may therefore

allow for standardized procedures for data acquisition as well as preprocessing pipelines for artifact removal given the reproducibility and reduced variance in the data. Despite the specificity of our considerations to the boundary of our laboratory, the results reported here with *compact* setup will not only be of interest to researchers approaching simultaneous EEG-fMRI recordings, but also may provide the foundational groundwork for developing standardized procedures for future EEG-fMRI research.

Acknowledgements

This work has been realized thank to the support from the Provincia autonoma di Trento and the Fondazione Cassi di Risparmio di Trento e Rovereto. We would like to thank Dr Mazza (University of Trento) for her guidance in the interpretation and quality assessment of human data. We are indebted to Dr. Stoermer (Brain Products) for invaluable discussions and for reviewing an earlier version of the manuscript. We are grateful to the MR-staff of the LNIF laboratory, for their assistance acquiring human data. We also want to thank Marco Buiatti, Jens Schwarzbach and Michele Furlan for their help on early evaluations of our MR-compatible EEG equipment.

References

Allen, P. J., Josephs, O., & Turner, R. (2000). A method for removing imaging artifact from continuous EEG recorded during functional MRI. *NeuroImage*, *12*(2), 230–239. http://doi.org/10.1006/nimg.2000.0599

Anami, K., Mori, T., Tanaka, F., Kawagoe, Y., Okamoto, J., Yarita, M., … Saitoh, O. (2003). Stepping stone sampling for retrieving artifact-free electroencephalogram during functional magnetic resonance imaging. *NeuroImage*, *19*(2 Pt 1), 281–295.

Assecondi, S., Ferrari, P., Jovicich, J., 2013. A compact setup to improve the quality of EEG data recorded during fMRI. 21st Annual Meeting & Exhibition of the International Society for Magnetic Resonance in Medicine, Salt Lake City, Utah, USA.

*Brainard DH. The psychophysics toolbox. Spat Vis 1997, **10**(4):433–436*

Chowdhury, M. E. H., Mullinger, K. J., & Bowtell, R. (2015). Simultaneous EEG-fMRI: evaluating the effect of the cabling configuration on the gradient artefact. *Physics in Medicine and Biology*, *60*(12), N241–250. http://doi.org/10.1088/0031-9155/60/12/N241

Debener, S., Mullinger, K. J., Niazy, R. K., & Bowtell, R. W. (2008). Properties of the ballistocardiogram artefact as revealed by EEG recordings at 1.5, 3 and 7 T static magnetic field strength. *International Journal of Psychophysiology: Official Journal of the International Organization of Psychophysiology*, *67*(3), 189–199. http://doi.org/10.1016/j.ijpsycho.2007.05.015

Delorme, A., & Makeig, S. (2004). EEGLAB: an open source toolbox for analysis of single-trial EEG dynamics including independent component analysis. *Journal of Neuroscience Methods*, *134*(1), 9–21. http://doi.org/10.1016/j.jneumeth.2003.10.009

De Vos, M., Zink, R., Hunyadi, B., Mijovic, B., Van Huffel, S., & Debener, S. (2013). The quest for single trial correlations in multimodal EEG-fMRI data. *Conference Proceedings: ... Annual International Conference of the IEEE Engineering in Medicine and Biology Society. IEEE Engineering in Medicine and Biology Society. Annual Conference*, *2013*, 6027–6030. http://doi.org/10.1109/EMBC.2013.6610926

Ertl, M., Kirsch, V., Leicht, G., Karch, S., Olbrich, S., Reiser, M., … Mulert, C. (2010). Avoiding the ballistocardiogram (BCG) artifact of EEG data acquired simultaneously with fMRI by pulse-triggered presentation of stimuli. *Journal of Neuroscience Methods*, *186*(2), 231–241. http://doi.org/10.1016/j.jneumeth.2009.11.009

Felblinger, J., Debatin, J. F., Boesch, C., Gruetter, R., & McKinnon, G. C. (1995). Synchronization device for electrocardiography-gated echo-planar imaging. *Radiology*, *197*(1), 311–313. http://doi.org/10.1148/radiology.197.1.7568844

Friedman, L., & Glover, G. H. (2006). Report on a multicenter fMRI quality assurance protocol. *Journal of Magnetic Resonance Imaging: JMRI*, *23*(6), 827–839. http://doi.org/10.1002/jmri.20583

Garreffa, G., Carnì, M., Gualniera, G., Ricci, G. B., Bozzao, L., De Carli, D., … Maraviglia, B. (2003). Real-time MR artifacts filtering during continuous EEG/fMRI acquisition. *Magnetic Resonance Imaging*, *21*(10), 1175–1189.

Goldman, R. I., Stern, J. M., Engel, J., & Cohen, M. S. (2000). Acquiring simultaneous EEG and functional MRI. *Clinical Neurophysiology: Official Journal of the International Federation of Clinical Neurophysiology*, *111*(11), 1974–1980.

Hamandi, K., Salek-Haddadi, A., Fish, D. R., & Lemieux, L. (2004). EEG/functional MRI in epilepsy: The Queen Square Experience. *Journal of Clinical Neurophysiology: Official Publication of the American Electroencephalographic Society*, *21*(4), 241–248.

Herrmann, C. S., & Debener, S. (2008). Simultaneous recording of EEG and BOLD responses: a historical perspective. *International Journal of Psychophysiology: Official Journal of the International Organization of Psychophysiology*, *67*(3), 161–168. http://doi.org/10.1016/j.ijpsycho.2007.06.006

Hill, R. A., Chiappa, K. H., Huang-Hellinger, F., & Jenkins, B. G. (1995). EEG during MR imaging: differentiation of movement artifact from paroxysmal cortical activity. *Neurology*, *45*(10), 1942–1943.

Huster, R. J., Debener, S., Eichele, T., & Herrmann, C. S. (2012). Methods for simultaneous EEG-fMRI: an introductory review. *The Journal of Neuroscience: The Official Journal of the Society for Neuroscience*, *32*(18), 6053–6060. http://doi.org/10.1523/JNEUROSCI.0447-12.2012

Ives, J. R., Warach, S., Schmitt, F., Edelman, R. R., & Schomer, D. L. (1993). Monitoring the patient's EEG during echo planar MRI. *Electroencephalography and Clinical Neurophysiology*, *87*(6), 417–420.

Jenkinson, M. (2003). Fast, automated, N-dimensional phase-unwrapping algorithm. *Magnetic Resonance in Medicine*, *49*(1), 193–197. http://doi.org/10.1002/mrm.10354

Jezzard, P., & Balaban, R. S. (1995). Correction for geometric distortion in echo planar images from B0 field variations. *Magnetic Resonance in Medicine*, *34*(1), 65–73.

Jorge, J., Grouiller, F., Ipek, Ö., Stoermer, R., Michel, C. M., Figueiredo, P., … Gruetter, R. (2015). Simultaneous EEG-fMRI at ultra-high field: artifact prevention and safety assessment. *NeuroImage*, *105*, 132–144. http://doi.org/10.1016/j.neuroimage.2014.10.055

Kim, H.-C., Yoo, S.-S., & Lee, J.-H. (2015). Recursive approach of EEG-segment-based principal component analysis substantially reduces cryogenic pump artifacts in simultaneous EEG-fMRI data. *NeuroImage*, *104*, 437–451. http://doi.org/10.1016/j.neuroimage.2014.09.049

Laufs, H. (2008). Endogenous brain oscillations and related networks detected by surface EEG-combined fMRI. *Human Brain Mapping*, *29*(7), 762–769. http://doi.org/10.1002/hbm.20600

Laufs, H., Krakow, K., Sterzer, P., Eger, E., Beyerle, A., Salek-Haddadi, A., & Kleinschmidt, A. (2003). Electroencephalographic signatures of attentional and cognitive default modes in spontaneous brain activity fluctuations at rest. *Proceedings of the National Academy of Sciences of the United States of America*, *100*(19), 11053–11058. http://doi.org/10.1073/pnas.1831638100

Lavallee, C. F., Herrmann, C. S., Weerda, R., & Huster, R. J. (2014). Stimulus-response mappings shape inhibition processes: a combined EEG-fMRI study of contextual stopping. *PloS One*, *9*(4), e96159. http://doi.org/10.1371/journal.pone.0096159

Lemieux, L., Allen, P. J., Franconi, F., Symms, M. R., & Fish, D. R. (1997). Recording of EEG during fMRI experiments: patient safety. *Magnetic Resonance in Medicine*, *38*(6), 943–952.

Mandelkow, H., Halder, P., Boesiger, P., & Brandeis, D. (2006). Synchronization facilitates removal of MRI artefacts from concurrent EEG recordings and increases usable bandwidth. *NeuroImage*, *32*(3), 1120–1126. http://doi.org/10.1016/j.neuroimage.2006.04.231

Morrell, G. R. (2008). A phase-sensitive method of flip angle mapping. *Magnetic Resonance in Medicine*, *60*(4), 889–894. http://doi.org/10.1002/mrm.21729

Mulert, C., & Lemieux, L. (Eds.). (2010). *EEG - fMRI*. Berlin, Heidelberg: Springer Berlin Heidelberg. Retrieved from http://link.springer.com/10.1007/978-3-540-87919-0

Mullinger, K., Brookes, M., Stevenson, C., Morgan, P., & Bowtell, R. (2008a). Exploring the feasibility of simultaneous electroencephalography/functional magnetic resonance imaging at 7 T. *Magnetic Resonance Imaging*, *26*(7), 968–977. http://doi.org/10.1016/j.mri.2008.02.014

Mullinger K, Debener S, Coxon R, Bowtell R. Effects of simultaneous EEG recording on MRI data quality at 1.5, 3 and 7 tesla. Int J Psychophysiol. (2008b);67(3):178-88.

Mullinger, K. J., Yan, W. X., & Bowtell, R. (2011). Reducing the gradient artefact in simultaneous EEG-fMRI by adjusting the subject's axial position. *NeuroImage*, *54*(3), 1942–1950. http://doi.org/10.1016/j.neuroimage.2010.09.079

Müri, R. M., Felblinger, J., Rösler, K. M., Jung, B., Hess, C. W., & Boesch, C. (1998). Recording of electrical brain activity in a magnetic resonance environment: distorting effects of the static magnetic field. *Magnetic Resonance in Medicine*, *39*(1), 18–22.

Negishi, M., Pinus, B. I., Pinus, A. B., & Constable, R. T. (2007). Origin of the radio frequency pulse artifact in simultaneous EEG-fMRI recording: rectification at the carbon-metal interface. *IEEE Transactions on Bio-Medical Engineering*, *54*(9), 1725–1727. http://doi.org/10.1109/TBME.2007.891940

Nierhaus, T., Gundlach, C., Goltz, D., Thiel, S. D., Pleger, B., & Villringer, A. (2013). Internal ventilation system of MR scanners induces specific EEG artifact during simultaneous EEG-fMRI. *NeuroImage*, *74*, 70–76. http://doi.org/10.1016/j.neuroimage.2013.02.016

Odom, J. V., Bach, M., Barber, C., Brigell, M., Marmor, M. F., Tormene, A. P., … Vaegan, null. (2004). Visual evoked potentials standard (2004). *Documenta Ophthalmologica. Advances in Ophthalmology*, *108*(2), 115–123.

Odom, J. V., Bach, M., Brigell, M., Holder, G. E., McCulloch, D. L., Tormene, A. P., & Vaegan, null. (2010). ISCEV standard for clinical visual evoked potentials (2009 update). *Documenta Ophthalmologica. Advances in Ophthalmology*, *120*(1), 111–119. http://doi.org/10.1007/s10633-009-9195-4

Ritter, P., & Villringer, A. (2006). Simultaneous EEG-fMRI. *Neuroscience and Biobehavioral Reviews*, *30*(6), 823–838. http://doi.org/10.1016/j.neubiorev.2006.06.008

Robinson, S., & Jovicich, J. (2011). B0 mapping with multi-channel RF coils at high field. *Magnetic Resonance in Medicine*, *66*(4), 976–988. http://doi.org/10.1002/mrm.22879

Simultaneous EEG and fMRI - Markus Ullsperger, Stefan Debener - Oxford University Press. (n.d.). Retrieved November 21, 2015, from https://global.oup.com/academic/product/simultaneous-eeg-and-fmri-9780195372731?cc=it&lang=en&

Smith, S. M. (2002). Fast robust automated brain extraction. *Human Brain Mapping*, *17*(3), 143–155. http://doi.org/10.1002/hbm.10062

Smith, S. M., Jenkinson, M., Woolrich, M. W., Beckmann, C. F., Behrens, T. E. J., Johansen-Berg, H., … Matthews, P. M. (2004). Advances in functional and structural MR image analysis and implementation as FSL. *NeuroImage*, *23 Suppl 1*, S208–219. http://doi.org/10.1016/j.neuroimage.2004.07.051

Vanderperren, K., Mijović, B., Novitskiy, N., Vanrumste, B., Stiers, P., Van den Bergh, B. R. H., … De Vos, M. (2013). Single trial ERP reading based on parallel factor analysis. *Psychophysiology*, *50*(1), 97–110. http://doi.org/10.1111/j.1469-8986.2012.01405.x

Vulliemoz, S., Carmichael, D. W., Rosenkranz, K., Diehl, B., Rodionov, R., Walker, M. C., … Lemieux, L. (2011). Simultaneous intracranial EEG and fMRI of interictal epileptic discharges in humans. *NeuroImage*, *54*(1), 182–190. http://doi.org/10.1016/j.neuroimage.2010.08.004

Woolrich, M. W., Jbabdi, S., Patenaude, B., Chappell, M., Makni, S., Behrens, T., … Smith, S. M. (2009). Bayesian analysis of neuroimaging data in FSL. *NeuroImage*, *45*(1 Suppl), S173–186. http://doi.org/10.1016/j.neuroimage.2008.10.055

Worsley, K. J., Evans, A. C., Marrett, S., & Neelin, P. (1992). A three-dimensional statistical analysis for CBF activation studies in human brain. *Journal of Cerebral Blood Flow and*

Metabolism: Official Journal of the International Society of Cerebral Blood Flow and Metabolism, *12*(6), 900–918. http://doi.org/10.1038/jcbfm.1992.127

Zaitsev, M., Hennig, J., & Speck, O. (2004). Point spread function mapping with parallel imaging techniques and high acceleration factors: fast, robust, and flexible method for echo-planar imaging distortion correction. *Magnetic Resonance in Medicine*, *52*(5), 1156–1166. http://doi.org/10.1002/mrm.20261

Zeng, H., & Constable, R. T. (2002). Image distortion correction in EPI: comparison of field mapping with point spread function mapping. *Magnetic Resonance in Medicine*, *48*(1), 137–146. http://doi.org/10.1002/mrm.10200

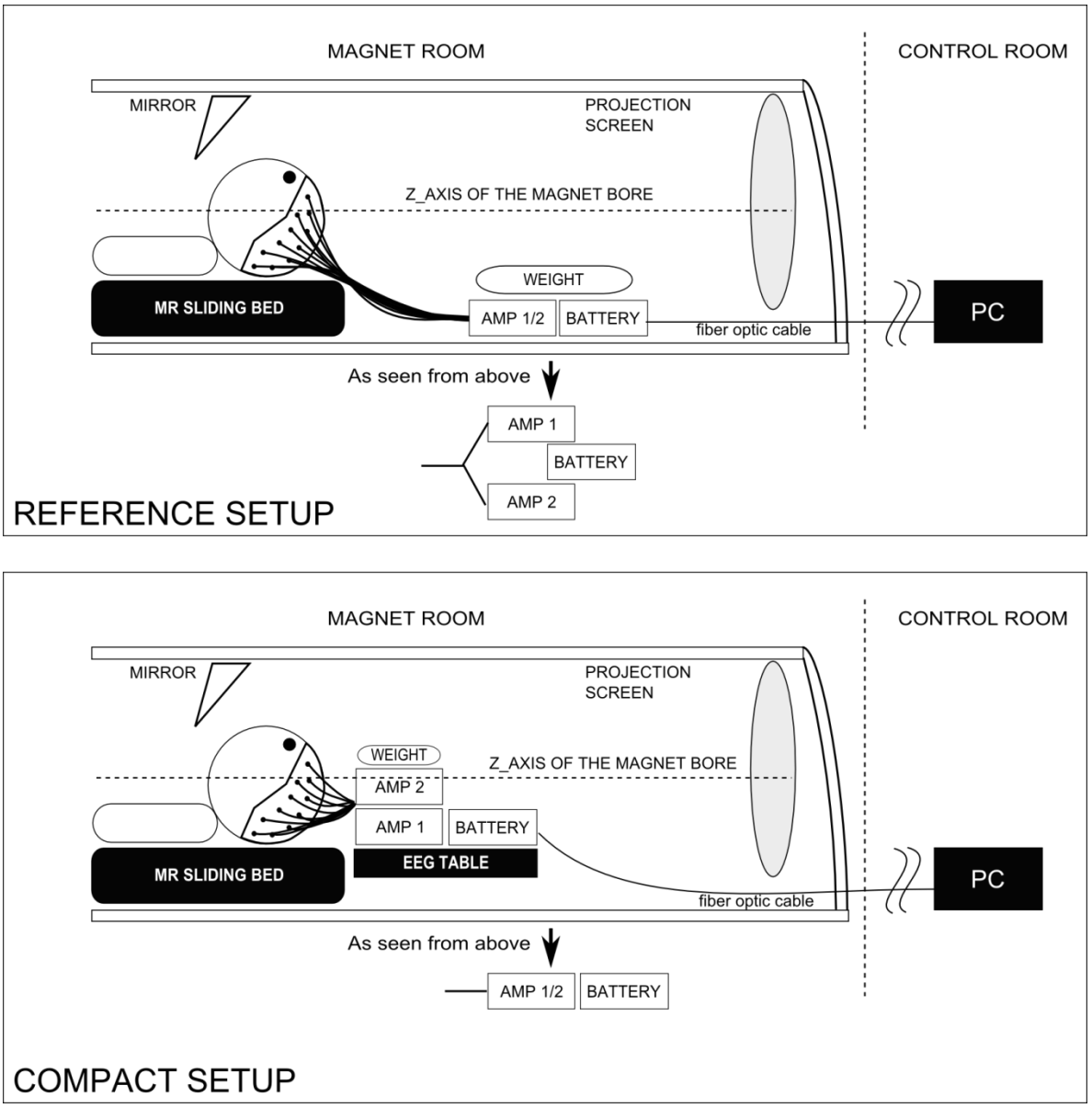

Figure 1: Schematic representation of the *reference* (top) and *compact* EEG setups (bottom).

See text for a detailed description.

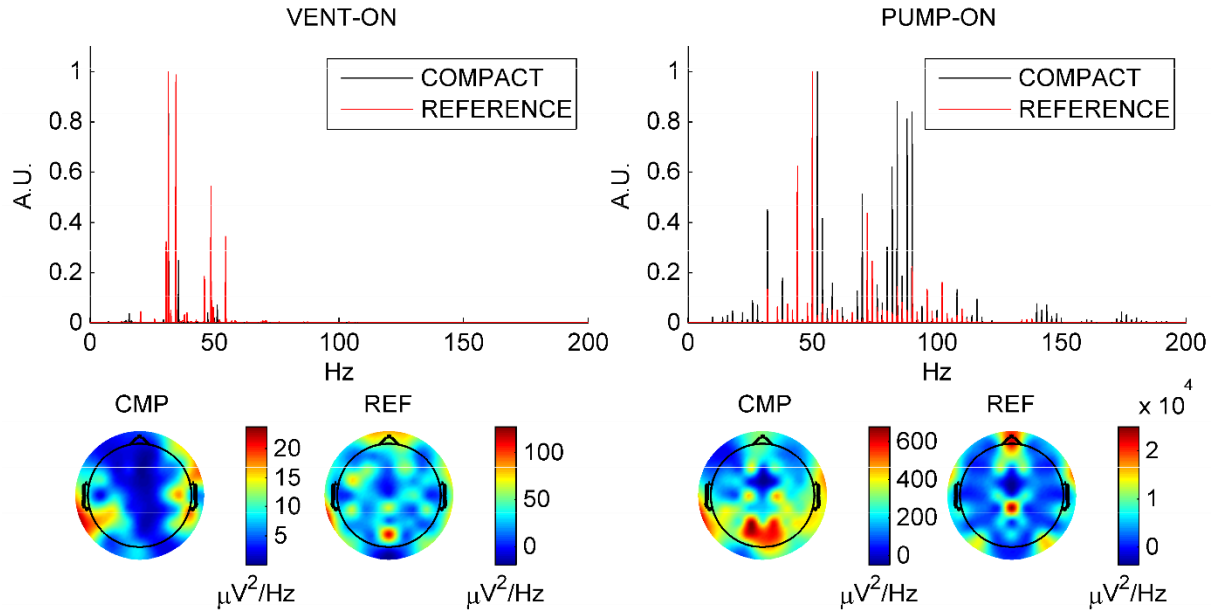

Figure 2: Phantom EEG sensitivity to environmental noise inside the magnet without concurrent MRI acquisition. Comparison of the EEG power spectral density (PSD, total power with sum over frequencies) profiles (upper row) and scalp maps (lower row, note scale differences), re-referenced to the ALL-OFF condition, for phantom recordings with the two experimental setups (*compact* and *reference*) during the VENT-ON (left side) and PUMP-ON (right side) conditions (see Table 2). The *compact* setup gives lower noise signals without concurrent MRI.

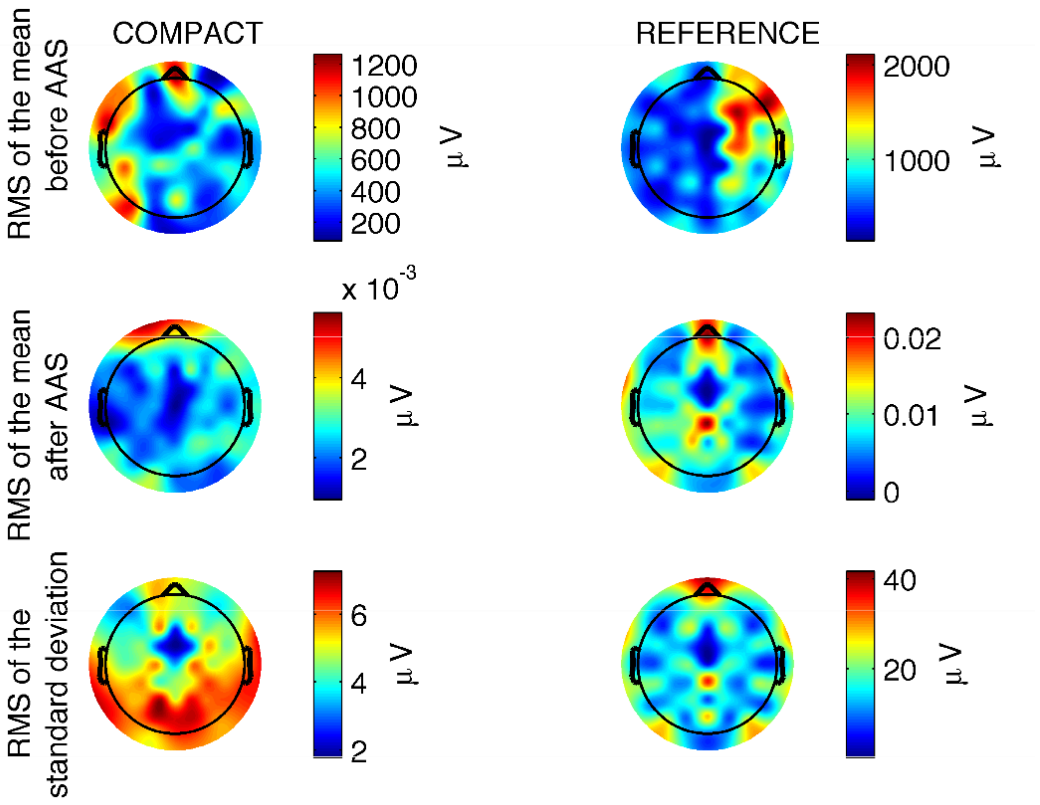

Figure 3: Phantom EEG signal noise during simultaneous MRI acquisition *(ALL-ON condition).*Phantom EEG map distribution of the RMS of the average artifact before and after AAS (upper and middle row, respectively). Standard deviations of the EEG signal noise during simultaneous EEG-fMRI recordings (lower row). Note the noise scale differences between the *compact* (left) and *reference* (right) setups. The *compact* setup gives lower EEG noise signal during concurrent EEG-fMRI.

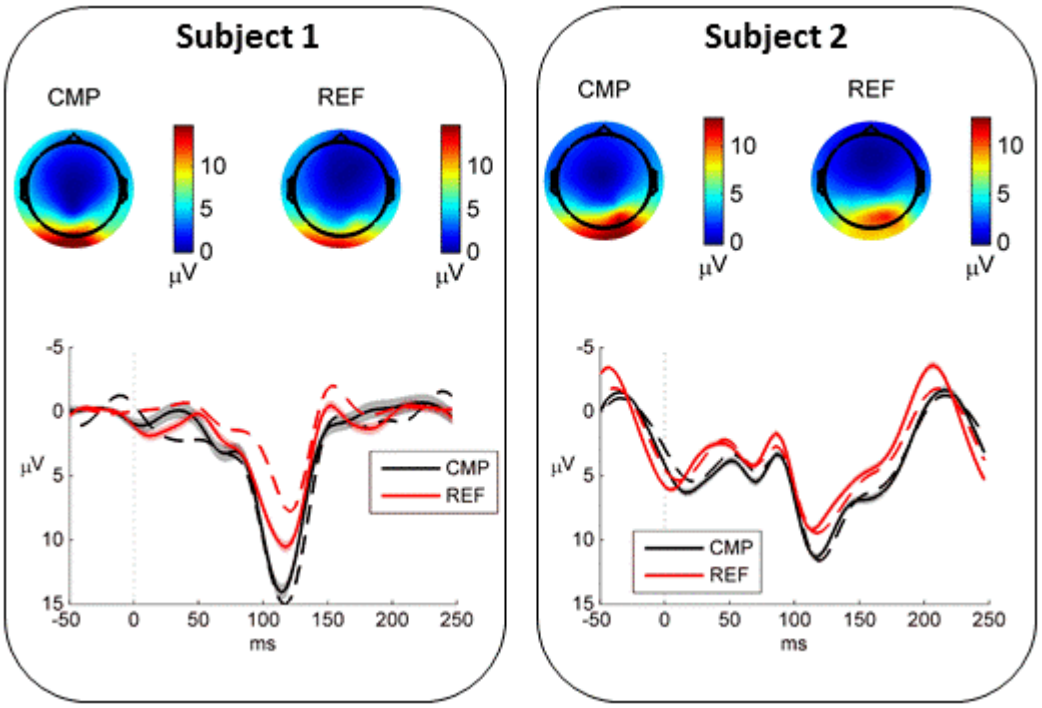

Figure 4: Effects of acquisition setup and environmental noise on ERP responses. Upper row: scalp distribution of the P100 (maximum positive peak around 100 ms) for the ALL-ON condition on the two subjects (CMP: compact, REF: reference). Lower row: Comparison of single-subject average ERP responses in four conditions: two acquisition setups (black for compact, CMP, and red for reference, REF) and two environmental noise conditions (thick line in darker color in ALL-ON condition, dashed lighter color for ALL-OFF condition). Error margins represent ERP standard error across trials. Human recordings are from each subject passively viewing a flashing checker-board. Both subjects show that the compact setup gives a higher effect size and is less sensitive to environmental noise.

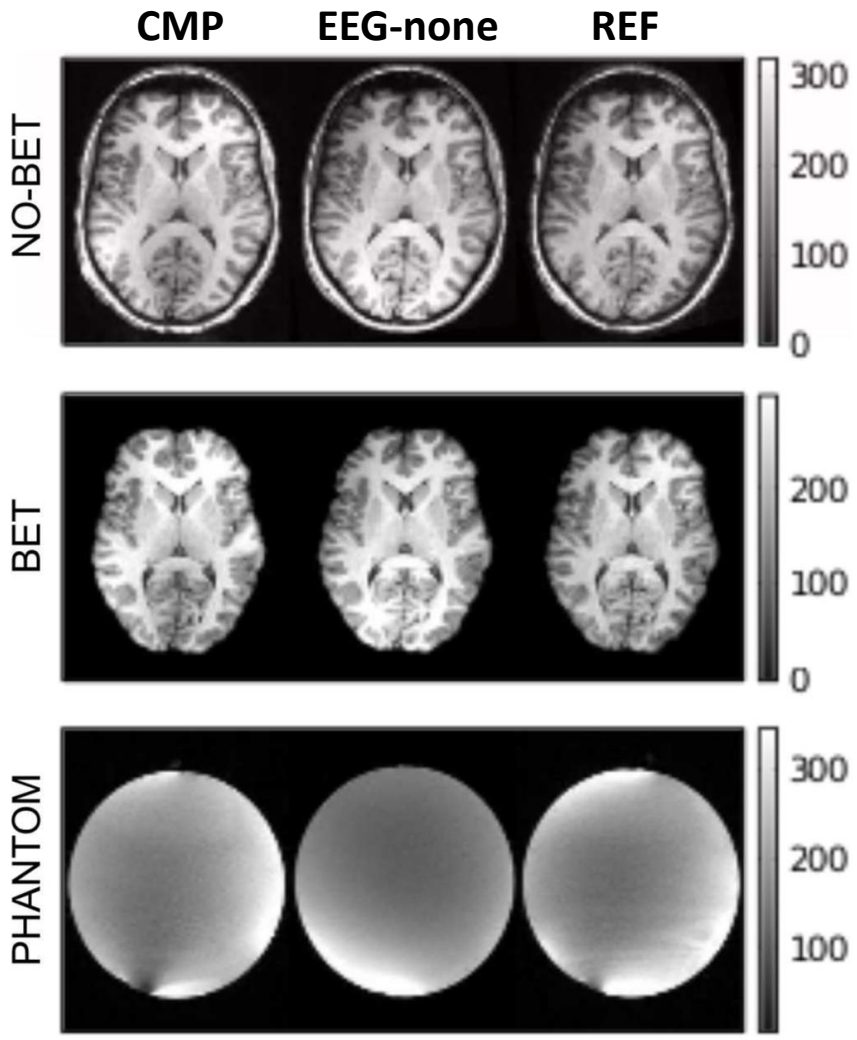

Figure 5: **Effects of EEG *compact* and *reference* setups on anatomical MRI.** Representative central axial anatomical MRI slice with (*compact* - CMP, *reference* - REF) and without concurrent EEG (EEG-none). Upper row: sample anatomical image. Middle row: brain extracted (BET) anatomical image. Lower row: anatomical phantom images. No mayor image distortion artifacts are visible on the structural images across the experimental setups. Intensity inhomogeneities in the structural images in both EEG-fMRI setups were stronger relative to EEG-none (Fig. 6).

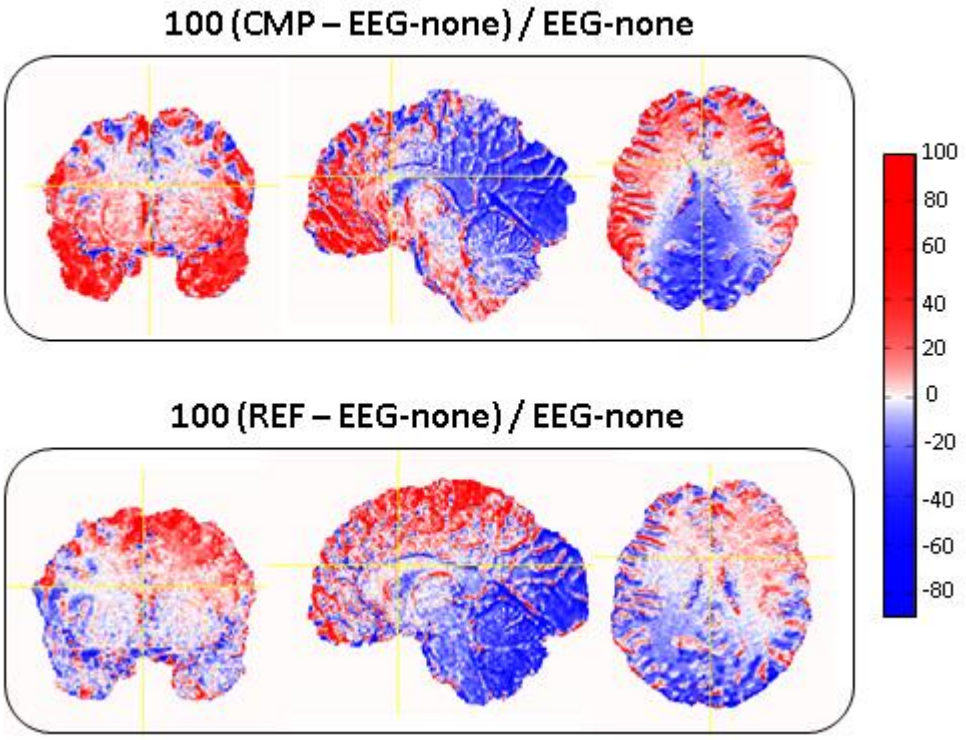

Figure 6: Anatomical intensity inhomogeneities in the compact (CMP, above) and reference (REF, below) EEG-fMRI setups relative to MRI without EEG (EEG-none). Percent difference maps of anatomical T1 intensity variations with respect to the EEG-none condition. Brain extracted data, color coded between -100% and +100%.

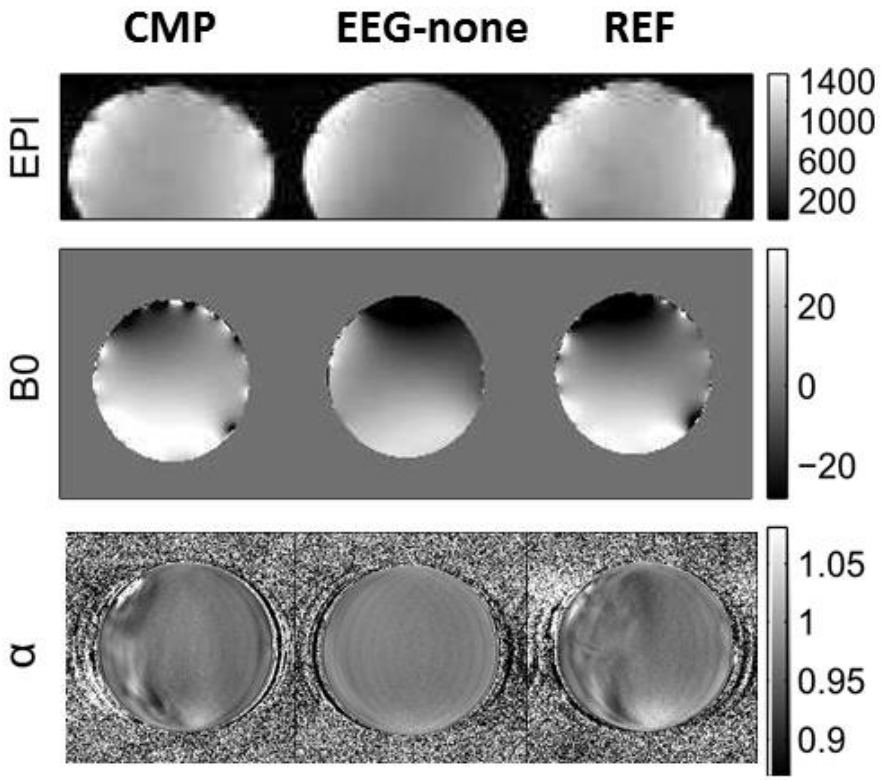

Figure 7: Phantom effects of EEG *compact* (CMP) and *reference* (REF) setups on functional MRI, B0 and flip angle homogeneity. Representative sagittal slices of functional (upper row), static field B_0 (middle row) and flip angle α (lower row) phantom recordings with (CMP or REF) and without concurrent EEG (EEG-none). The CMP and REF setups show both visible effects relative to the EEG-none condition.

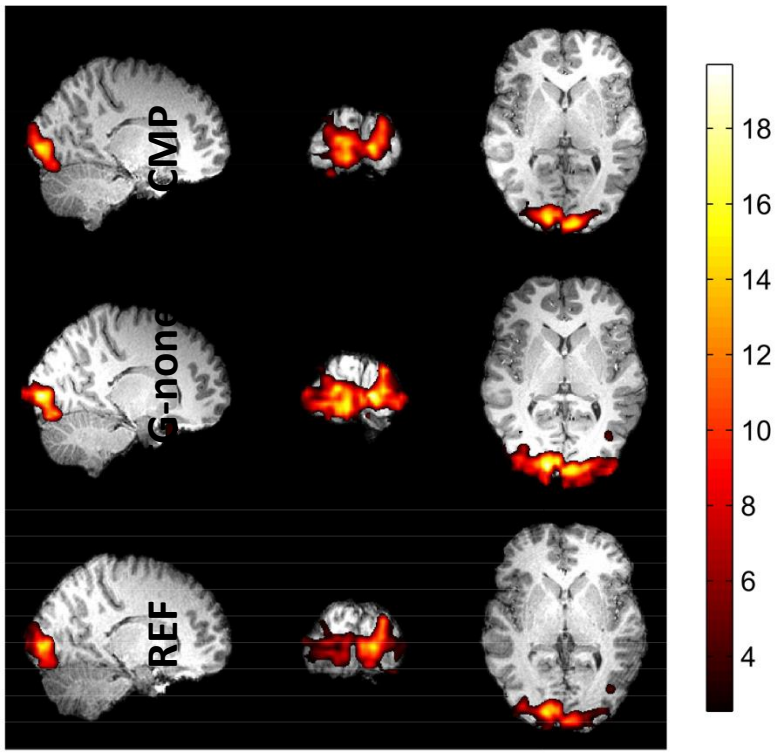

Figure 8: Effects of EEG *compact* and *reference* setups on concurrent fMRI activation. Sample human fMRI recordings (one subject, passive viewing of a flashing checker-board) with (*compact* (CMP), *reference* (REF)) and without concurrent EEG (EEG-none). Slices were selected in correspondence of the maximally activated voxel. Neither major artifacts nor qualitative differences are seen in the visual fMRI activation between the *compact* and *reference* setups.

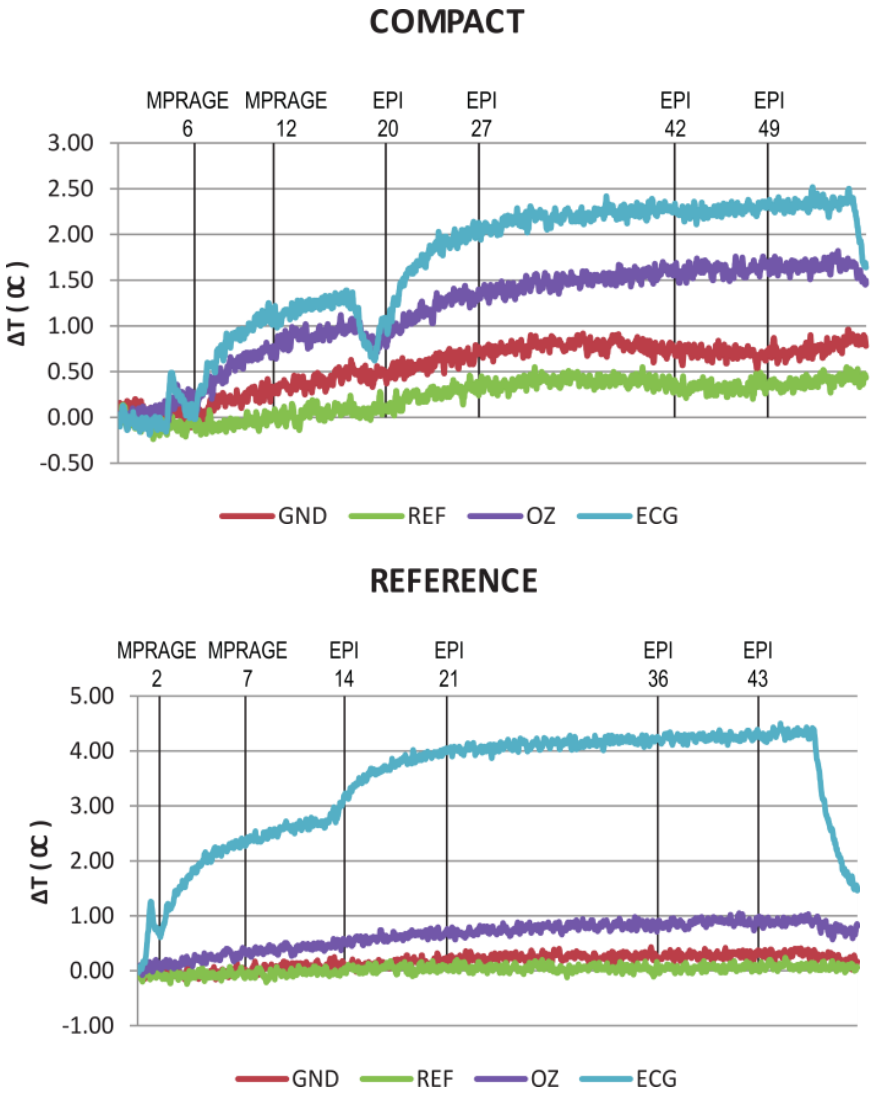

Figure 9: Effects of EEG *compact* and *reference* setups on phantom temperature measures. Relative temperature changes were measured near four electrodes (color coded) on a phantom as function of time during which different MRI were acquired. The numbers below the sequence labels represent the time, in minutes, at which each sequence started.

Table 1: Overview of the different EEG-fMRI experimental conditions, both for phantom (top) and human (bottom) experiments. EEG-full: whole EEG system in place and recording in magnet bore. EEG-amps: only the EEG amplifiers and battery pack placed in magnet bore and switched off. EEG-none: no EEG system present in magnet bore. During each session either EEG signals (S), functional MRI images (I) or both, were recorded. Additionally anatomical (M), maps of the static field (B_0) and maps of the flip angle (α) were acquired for each session. Temperature (T) was monitored throughout phantom EEG sessions.

Phantom Recordings				
Magnetic fields	Condition	Session		
		EEG-full	EEG-amps	EEG-none
STATIC	ALL-ON	S/T	-	-
	VENT-ON	S/T	-	-
	PUMP-ON	S/T	-	-
	ALL-OFF	S/T	-	-
IMG	ALL-ON	S/T/I	I	I
	VENT-ON	S/T/I	-	-
	PUMP-ON	S/T/I	-	-
	ALL-OFF	S/T/I	-	-
ADDITIONAL DATA		$M/B_0/\alpha$	$M/B_0/\alpha$	$M/B_0/\alpha$

Human Recordings				
Magnetic fields	Condition	Session		
		EEG-full	-	EEG-none
STATIC	ALL-ON	S	-	-
	ALL-OFF	S	-	-
IMG	ALL-ON	S/I	-	I
	ALL-OFF	S/I	-	-
ADDITIONAL DATA		$M/B_0/\alpha$	-	$M/B_0/\alpha$

Table 2: Overview of different experimental conditions evaluated for both human and phantom recordings. With human subjects, only the gray background conditions were considered.

Experimental conditions	**Cryogenic pump**	**Ventilation system**
ALL-ON	ON	ON
VENT-ON	OFF	ON
PUMP-ON	ON	OFF
ALL-OFF	OFF	OFF

Table 3: Effects of compact and reference EEG experimental setups on fMRI signal stability**.** The means μ of the following quantities are reported: average signal intensity (mean), Signal-to-Noise Ratio (SNR), Signal- to-Fluctuation Noise Ratio (SFNR), standard deviation (stdev), percentage fluctuation and drift. For the EEG-none condition (baseline from the previous three years) the standard deviation σ is also reported.

FBIRN stability	**CMP(μ)**	**REF (μ)**	**EEG-none (μ ± σ)**
mean	942	980	795 ± 29
SNR	204.72	199.83	225.17 ± 19.28
SFNR	193.34	188.26	215.03 ± 20.81
Stdev	1.33	1.68	1.33 ± 4.33
Fluctuation (%)	0.14	0.17	0.17 ± 0.55
Drift (%)	0.22	0.20	0.19 ± 0.32

Table 4: Comparison of phantom MRI spatial inhomogeneities in static magnetic field (B0) and normalized flip angle maps (α) across experimental setups (compact EEG-fMRI: CMP; reference EEG-fMRI: REF, no EEG equipment: EEG-none). The comparison is based on paired t-test across setups using as uniformity the standard deviations of the B0 or flip angle maps within the phantom images across phantom slices. N.S.: not significant difference.

	Spatial MRI uniformity differences (p-values)		
	CMP vs. EEG-none	**REF vs. EEG-none**	**REF vs. CMP**
B_0	1.37 e-5	4.58 e-6	n.s.
α	5.69 e-24	2.06 e-23	6.70 e -13

Table 5: Proton NMR resonance frequencies (ν) and corresponding half wavelengths (λ/2) for different static field strengths.

B_0 (T)	ν (MHz)	λ/2 (cm)
1.5	63.87	234.85
3	127.74	117.43
4	170.32	88.07
7	298.06	50.33